Effects of vibrational excitation on multidimensional tunneling: General study and proton tunneling in tropolone

Shoji Takada and Hiroki Nakamura

Division of Theoretical Studies, Institute for Molecular Science, Myodaiji, Okazaki 444, Japan

Tunneling energy splittings of vibrationally excited states are calculated quantum mechanically using several models of two-dimensional symmetric double well potentials. Various effects of vibrational excitation on tunneling are found to appear, depending on the topography of potential energy surface; the symmetry of the mode coupling plays an essential role. Especially, oscillation of tunneling splitting with respect to vibrational quantum number can occur and is interpreted by a clear physical picture based on the semiclassical theory formulated recently [Takada and Nakamura, J. Chem. Phys. **100**, 98 (1994)]. The *mixed tunneling* in the C region found there allows the wave functions to have nodal lines in classically inaccessible region and can cause the suppression of the tunneling. The above analysis is followed by the interpretation of recent experiments of proton tunneling in tropolone. *Ab initio* molecular orbital calculations are carried out for the electronically ground state. A simple three-dimensional model potential is constructed and employed to analyze the proton tunneling dynamics. Some of the experimentally observed intriguing features can be explained by the typical mechanisms discussed above. © *1995 American Institute of Physics.*

I. INTRODUCTION

Multidimensionality of quantum mechanical tunneling has been well recognized to be important and has attracted much attention in various fields of science.[1–15] Recently, we have developed a general Wentzel–Kramers–Brillouin (WKB) theory of multidimensional tunneling for energy splitting in double well potential and have found the following interesting features.[16,17] (1) There exist two types of tunneling (pure tunneling and mixed tunneling). (2) No tunneling path can be defined in the case of mixed tunneling. (3) Vibrational excitation can suppress tunneling because of the mixed tunneling. The mixed tunneling is such a tunneling that classical motion is allowed in one or more directions in the multidimensional space. The tunneling which usually occurs to our minds is the pure tunneling in which classical motion is not allowed in any direction. It should be noted that the wave functions in the case of mixed tunneling have nodal structures in the classically inaccessible regions.

One typical example of multidimensional tunnelings studied so far is the proton tunneling in malonaldehyde.[18–21] Two or three relevant coordinates are chosen intuitively to derive the reaction surface Hamiltonian, and the reliable *ab initio* molecular orbital (MO) calculations have been carried out. The energy splitting E_0 calculated based on this Hamiltonian agrees reasonably well with experiment.[21] Using the three-dimensional reaction surface Hamiltonian, Shida *et al.* obtained 9 cm^{-1} for the vibrationally ground state energy splitting,[19] which is about 40% of the experimental value. Taking account of the accuracy of the potential energy surface (PES), we believe this to be quite satisfactory. On the other hand, one-dimensional models both along the intrinsic reaction coordinate (IRC) and along the straight line path underestimate ΔE_0 by orders of magnitude.

In contrast to the case of malonaldehyde, tropolone presents a more interesting, but more complicated problem associated with the mixed tunneling mentioned above. Proton tunneling of tropolone has been investigated extensively as a typical interesting system of multidimensional tunneling,[22–35] although the data are still not enough to clarify the mechanisms. As is shown in Fig. 1, tropolone has two equivalent potential minima, between which the proton tunneling occurs. In particular, for the electronically first excited state $\tilde{A}\ {}^1B_2$,[22–29] the tunneling energy splittings $\Delta E_{\mathbf{n}}$ of vibrationally excited states (**n** represents vibrational quantum numbers collectively) have been measured by Tomioka *et al.*,[24] Redington *et al.*,[25] and Sekiya *et al.*[27] The most interesting finding among them is that there are the following three kinds of vibrational modes with respect to the effects of the excitation on tunneling; (1) those which do not affect the tunneling, (2) those which promote the tunneling, and (3) those which suppress the tunneling. Needless to say, if there is no coupling between the tunneling coordinate and the coordinate transversal to it, the vibrational excitation in the latter does not affect energy splitting. This corresponds to the first type. When there is a coupling between the two coordinates, it is natural to expect from the analogy with the one-dimensional case that the vibrational excitation promotes the tunneling. However, the experimental findings clearly show that the real proton tunneling is not so simple. This fact nicely exemplifies the complexity of multidimensional tunneling. The following interesting questions arise: Under what conditions does vibrational excitation suppress the tunneling? What can we learn about the PES from data on tunneling splittings? Can we observe the *mixed tunneling*. A main purpose of this paper is to answer these questions.

Our present strategy to investigate these problems is as follows. We first investigate the tunneling energy splittings of vibrationally excited states using several typical model potentials. Both the exact quantum mechanical calculations and the calculations based on the adiabatic and sudden approximations are carried out. Depending on the topography
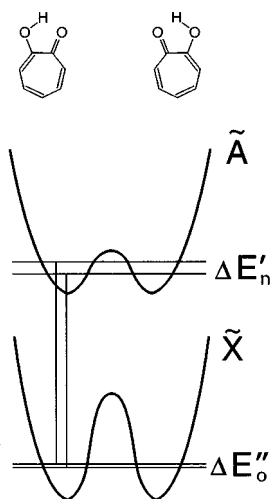
FIG. 1. Tropolone molecule and its schematic potential curve.

of PES, vibrational excitation was found to either promote or suppress the tunneling. Semiclassical theory turns out to nicely interpret these numerical results. Basically, the mixed tunneling plays an essential role in suppression and oscillation of energy splitting against vibrational excitation. Furthermore, the mechanism of the monotonic decrease of energy splitting is made clear. Second, the *ab initio* MO calculations have been carried out to clarify which kind of model PES actually corresponds to the proton tunneling of tropolone. This MO study does not aim at obtaining the accurate quantitative description of PES but at acquiring some information on the topography of PES. On the basis of these results, many of the available experimental data on tropolone are interpreted finally. It becomes clear that the symmetry of the coupling is one of the most important factors.

Since it is not easy to understand the characteristics of multidimensionality only by the quantum mechanical calculations, semiclassical theory is relied on to elucidate the physical picture of multidimensional tunneling. Our newly developed WKB theory mentioned above can be usefully utilized to analyze the numerical results obtained in the present work. For instance, this theory can predict oscillatory change of energy splitting with respect to vibrational quantum number, which has never been observed to the authors' knowledge. Thus, it is an especially interesting question whether this oscillation coming from mixed tunneling is *observable* or not in real molecules. Finally, it should be noted that this WKB theory can be applied equally to the tunneling of vibrationally excited states; the famous instanton theory is applicable only to the ground state,[4,5,15] although there is a trial to use the instantonlike treatment for vibrationally excited states.[36]

This paper is organized as follows. The general WKB theory of multidimensional tunneling and the adiabatic and sudden approximations used in the subsequent sections are briefly outlined in Sec. II. In Sec. III, the tunneling energy splittings of vibrationally excited states are numerically estimated with use of several typical model potentials and are analyzed by the WKB theory and the adiabatic and sudden

approximations. Section IV discusses proton tunneling of tropolone: (1) The *ab initio* MO calculations are performed for the electronically ground state of tropolone, and (2) with use of these calculations and the model studies of Sec. III, the experimentally observed interesting features are qualitatively interpreted. Concluding remarks are given in Sec. V.

II. THEORY OF MULTIDIMENSIONAL TUNNELING

For later convenience, we give a brief overview of the recently formulated general WKB theory,[16,17] and the adiabatic and sudden approximations. Here we confine ourselves, for simplicity, to the tunneling in two-dimensional symmetric double well potential (SDWP).

The Hamiltonian is assumed to be

$$H(x,y) = -\frac{\hbar^2}{2}\left(\frac{\partial^2}{\partial x^2} + \frac{\partial^2}{\partial y^2}\right) + V(x,y), \tag{1}$$

where the mass-scaled coordinates (x and y) are used. The tunneling energy splitting ΔE in SDWP can be calculated by using Herring's formula[37,16]

$$\Delta E = \hbar^2 \int_\Sigma d\sigma [\Psi^L \nabla \Psi^R - \Psi^R \nabla \Psi^L], \tag{2}$$

where the surface Σ divides the whole space into two equivalent regions and $\Psi^L(\Psi^R)$ is the wave function localized in the left (right) well defined by the symmetric (antisymmetric) linear combination of the quasidegenerate eigenstates. This formula gives a useful framework to calculate the energy splitting. For example, in the case of one-dimensional SDWP, the splitting can be expressed explicitly under the WKB approximation as,[38]

$$\Delta E = \frac{\hbar \omega}{\pi} e^{-\Theta}, \tag{3}$$

where ω is the frequency at local minima and the Gamow factor Θ is defined by

$$\Theta = \frac{1}{\hbar}\left|\int_{x_-}^{x_+} p\, dx\right|. \tag{4}$$

Here $x_\pm$ represent the classical turning points on the potential barrier and p is the momentum defined by $\sqrt{2[E - V(x)]}$.

A. General WKB theory

Recently, we have developed a WKB theory of multidimensional tunneling,[16,17] which can provide us with a clear conceptual understanding of the multidimensionality. The theory was formulated by solving the following basic problems: (i) construction of the semiclassical eigenfunction in classically allowed region according to the Maslov theory,[39] (ii) its connection to the wave function in the classically inaccessible region, and (iii) propagation of the latter into the deep tunneling region. It became clear that there exist two distinct tunneling regions: C region where action is complex and I region where action is pure imaginary.[40] Tunneling in these regions is qualitatively quite different from each other; in the I region the tunneling path can be defined by a certain
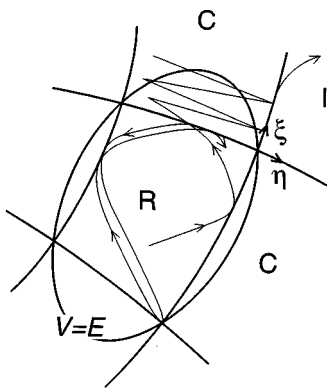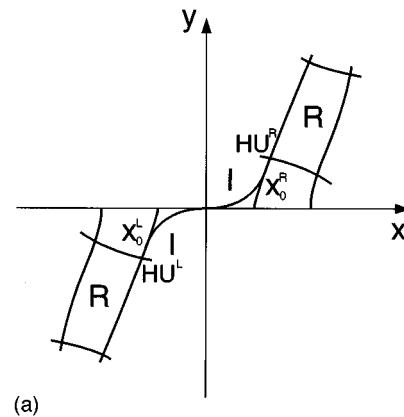
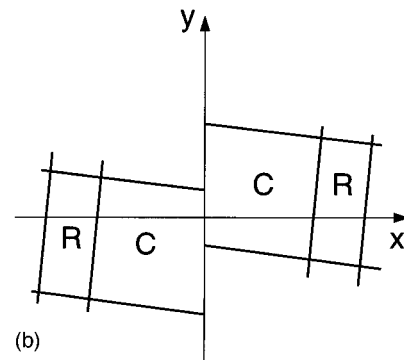FIG. 2. Schematic picture of tunneling region around a well.

classical trajectory on the inverted potential, while in the C region there is no unique path and the Huygens type wave propagation should be applied.

Figure 2 schematically shows the physical picture of tunneling obtained by the above general theory. The classical trajectories comprising a quantum eigenstate are confined within the distorted rectangular region (called R region hereafter), although the much wider region is energetically allowed (see the oval region bounded by $V=E$ in Fig. 2). Tunneling proceeds first to the C region where the motion in ξ direction is nonclassical (tunneling), while the motion in η direction is still classical. Thus, we call this type of tunneling "*mixed tunneling*." At the boundary between the C region and I region, part of the tunneling wave enters into the I region where no classical motion is allowed in any direction. This conventional type of tunneling is called "*pure tunneling*." One of the most outstanding differences between one-dimensional and multidimensional tunneling is the existence of mixed tunneling. Table I summarizes the characteristics of the tunneling in each region. It should be noted that the wave function in the C region has nodal lines, but that in the I region does not. This plays an important role in the effects of vibrational excitation on tunneling, as is discussed later.

Global feature of multidimensional tunneling is determined by the relative location of the two wells. Figures 3 illustrates two typical cases. Figure 3(a) depicts the case that

FIG. 3. Schematic picture of tunneling regions in the case of antisymmetric mode coupling. (a) Case of modest ω_y and γ, in which I region plays the essential role. x_0 are the points for the tunneling path (solid line) depart from the caustic curve. (b) Case of small coupling, in which C region plays a key role. Tunneling path cannot be defined.

after a short journey in the C region the wave propagates into the I region and the overall tunneling is characterized by the pure tunneling along the path running from $\mathbf{x}_0^L$ to $\mathbf{x}_0^R$. To obtain the energy splitting, the Gamow factor is calculated first along the caustics from HU^L to $\mathbf{x}_0^L$, then along the tunneling path from $\mathbf{x}_0^L$ to $\mathbf{x}_0^R$, and finally along the caustics from $\mathbf{x}_0^R$ to HU^R. See Eq. (4.14) of paper I, for instance. On the other hand, in Fig. 3(b) tunneling mainly proceeds through the C region and no tunneling path can be defined. See also

TABLE I. Characteristics of multidimensional tunneling obtained by the WKB theory (Ref. 16).

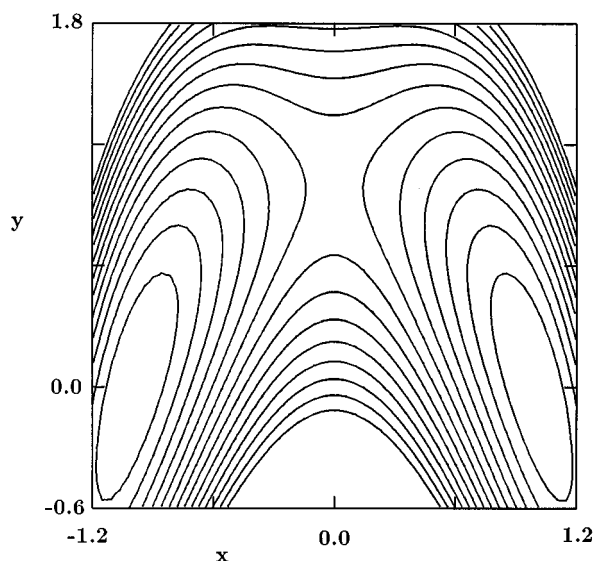|		WKB wave function	Characteristics
	R	$\Psi_{\mathbf{n}}=\Sigma_{\nu=1}^4(\rho_\nu)^{1/2}\exp[(i/\hbar)W_\nu]$	Classically allowed Nodal pattern
	C	$\Psi_{\mathbf{n}}=\Sigma_\pm(\rho_\pm)^{1/2}\exp[(i/\hbar)(\pm W_R+iW_I)]$	Mixed tunneling $\begin{pmatrix}\text{Tunneling in }\xi\text{ direction}\\\text{Classical in }\eta\text{ direction}\end{pmatrix}$ No tunneling path Nodal lines
	I	$\Psi_{\mathbf{n}}=\rho^{1/2}\exp[-(1/\hbar)W_I]$	Pure tunneling (No classical motion) Tunneling path =Classical traj. on $-V(x)$ No nodal line

FIG. 4. Contours of the symmetric mode coupling (SMC) potential [Eq. (19)] for the parameters $(\omega_y, \alpha) = (0.5, 1)$. The interval of contours is 0.02 and the contours with the energy higher than 0.28 are omitted.

Figs. 6 of paper I. We can straightforwardly generalize this concept to the case of more than two dimensions. There naturally appear many different kinds of C regions.

B. Adiabatic approximation

In the study of multidimensional tunneling, many versions of adiabatic approximation have been proposed[6–8,10] such as the slow flip approximation[6] and Marcus–Coltrin's path.[10]

For the moment let us focus our attention on the tunneling in a two-dimensional SDWP like the one shown in Fig. 4. The Hamiltonian is taken to be the same as Eq. (1). If we can assume that the frequency ω_x in x direction near the potential minimum is much smaller than that (ω_y) in y direction, then the total wave function can be expressed as,

$$\Psi_{\pm, n_x n_y}(x, y) = \phi_{\pm, n_x n_y}(x) \chi_{n_y}(y; x), \tag{5}$$

where $\pm$ specifies the parity with respect to y axis. The adiabatic bases χ_{n_y} are the solutions of

$$\left[-\frac{\hbar^2}{2} \frac{\partial^2}{\partial y^2} + V(x, y) \right] \chi_{n_y}(y; x) = \epsilon_{n_y}(x) \chi_{n_y}(y; x). \tag{6}$$

Inserting Eq. (5) into the Schrödinger equation and neglecting the derivative of χ_{n_y} with respect to x, we obtain

$$\left[-\frac{\hbar^2}{2} \frac{\partial^2}{\partial x^2} + \epsilon_{n_y}(x) \right] \phi_{\pm, n_x n_y}(x) = E_{\pm, n_x n_y}(x) \phi_{\pm, n_x n_y}(x). \tag{7}$$

Since this is a one-dimensional Schrödinger equation, the expression for energy splitting can be obtained as

$$\Delta E_{n_x n_y} = \Delta E_{n_x}^{1D}[\epsilon_{n_y}(x)], \tag{8}$$

where $\Delta E_{n_x}^{1D}[\epsilon_{n_y}(x)]$ is the one-dimensional formula of energy splitting given by Eq. (3), in which the potential $V(x)$ is replaced by the renormalized potential $\epsilon_{n_y}(x)$.

It should be noted that this treatment depends on the coordinate system and cannot be very legitimate. In chemical problems the intrinsic reaction coordinate (IRC)[41] is often employed as the adiabatic coordinate and the one-dimensional problem along IRC with the potential renormalized by the transversal vibrational energy is dealt with. This does not cause a serious difference from the above treatment at least in qualitative arguments, we simply use Eq. (8) as the adiabatic approximation in this paper.

C. Sudden approximation

We consider again the two-dimensional SDWP like the one shown in Fig. 4. The Hamiltonian is the same as Eq. (1) but now we assume that the frequency ω_y is much smaller than ω_x. Then, the eigenfunction can be written as

$$\Psi_{\pm, n_x n_y}(x, y) = \phi_{\pm, n_x n_y}(y) \chi_{\pm, n_x}(x; y), \tag{9}$$

where the adiabatic bases $\xi_{\pm, n_x}$ and the coefficient functions $\phi_{\pm, n_x, n_y}$ are defined in the analogous way to the previous subsection by,

$$\left(-\frac{\hbar^2}{2} \frac{\partial^2}{\partial x^2} + V(x, y) \right) \chi_{\pm, n_x}(x; y) = \epsilon_{\pm, n_x}(y) \chi_{\pm, n_x}(x; y), \tag{10}$$

$$\left(-\frac{\hbar^2}{2} \frac{\partial^2}{\partial y^2} + \epsilon_{\pm, n_x}(y) \right) \phi_{\pm, n_x n_y}(y) = E_{\pm, n_x n_y}(y) \phi_{\pm, n_x n_y}(y). \tag{11}$$

Since ϕ is not directly related to tunneling, we may approximate Eq. (11) by the separable equation,

$$\left(-\frac{\hbar^2}{2} \frac{\partial^2}{\partial y^2} + V(x_{min}, y) \right) \phi_{n_y}(y) = E'_{n_y}(y) \phi_{n_y}(y), \tag{12}$$

where x_{min} is x coordinate of the potential minimum. Taking symmetric and antisymmetric linear combinations of $\Psi_{\pm, n_x, n_y}$ we can obtain the localized wave functions as

$$\Psi_{n_x n_y}^L(x, y) = \phi_{n_y}(y) \chi_{n_x}^L(x; y) \tag{13}$$

and

$$\Psi_{n_x n_y}^R(x, y) = \phi_{n_y}(y) \chi_{n_x}^R(x; y). \tag{14}$$

Inserting these into Herring's formula (2), we obtain the final expression,

$$\Delta E_{n_x n_y} = \int_{x=0} dy \, \phi_{n_y}^2(y) \left[\hbar^2 \left(\chi_{n_x}^L(x; y) \frac{\partial \chi_{n_x}^R(x; y)}{\partial x} \right. \right.$$
$$\left. \left. - \chi_{n_x}^R(x; y) \frac{\partial \chi_{n_x}^L(x; y)}{\partial x} \right) \right]$$
$$= \int dy \, \phi_{n_y}^2(y) \Delta E_{n_x}^{1D}(y). \tag{15}$$

This is similar to the Franck–Condon approximation: Tunneling in x direction occurs at each fixed value of y, creating

the energy splitting $\Delta E_{n_x}^{\text{1D}}(y)$. The total energy splitting is obtained by averaging $\Delta E_{n_x}^{\text{1D}}(y)$ over y with the weight factor $\phi_{n_y}^2(y)$. It should be noted that this expression also depends on the definition of coordinate system. Several different kinds of formulations based on the same idea have been proposed so far in various fields of science.[7,11-13]

III. PROMOTION AND SUPPRESSION OF TUNNELING—TYPICAL MODELS

In this section, several typical model potentials are introduced to elucidate the mechanisms of promotion and suppression of tunneling by vibrational excitation. The tunneling energy splittings of vibrationally excited states are calculated not only exactly, but also approximately using the adiabatic and sudden approximations. The WKB theory summarized in the previous section can be usefully utilized to interpret the results. The model potential systems chosen so as to represent typical cases can actually be classified by their symmetries with respect to the coupling between the tunneling coordinate and the transversal coordinate. As will be shown, useful information on PES can be extracted from the experimental data with use of this symmetry consideration.

Exact quantum mechanical calculations have been carried out by using the discrete variable representation (DVR) method[42] with 70×70 grids. Results given here were confirmed to be accurate (at least) up to the figures given in the tables.

A. Case of symmetric mode coupling

Let us start with the Hamiltonian,

$$\tilde{H} = -\frac{\hbar^2}{2m_x}\frac{\partial^2}{\partial \tilde{x}^2} - \frac{\hbar^2}{2m_y}\frac{\partial^2}{\partial \tilde{y}^2} + \frac{m_x \tilde{\omega}_x^2}{8\tilde{x}_0^2}(\tilde{x} - \tilde{x}_0)^2(\tilde{x} + \tilde{x}_0)^2$$
$$+ \tfrac{1}{2} m_y \tilde{\omega}_y^2 [\tilde{y} + \tilde{\alpha}(\tilde{x}^2 - \tilde{x}_0^2)]^2, \tag{16}$$

where m_x, m_y, $\tilde{\omega}_x$, $\tilde{\omega}_y$, $2\tilde{x}_0$, and $\tilde{\alpha}$ are mass in x direction, mass in y direction, frequency in x direction, frequency in y direction, distance between two minima, and coupling strength, respectively. Without loss of generality, the Schrödinger equation

$$(\tilde{H} - \tilde{E})\tilde{\Psi} = 0 \tag{17}$$

can be scaled in such a way that all quantities become dimensionless. Introducing the following dimensionless quantities:

$$x = \frac{\tilde{x}}{\tilde{x}_0},$$

$$y = \frac{\tilde{y}}{\tilde{x}_0}\sqrt{\frac{m_x}{m_y}},$$

$$\omega_y = \frac{m_y \tilde{\omega}_y}{m_x \tilde{\omega}_x},$$

$$g = \frac{\hbar}{m_y \tilde{\omega}_x \tilde{x}_0^2}, \tag{18}$$
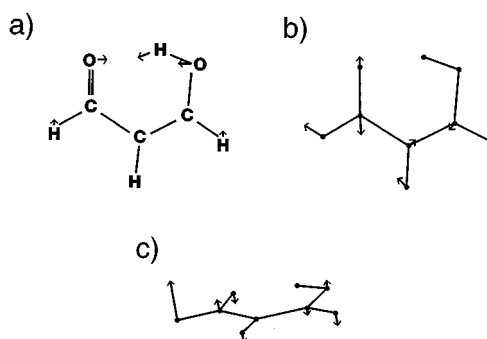

FIG. 5. Various modes coupled to the hydrogen tunneling mode in the case of malonaldehyde. (a) In-plane scissors like mode corresponding to the SMC model, (b) in-plane antisymmetric C–O stretching mode corresponding to the ASMC model, (c) out-of-plane wagging motion corresponding to the Sqz model.

$$E(\text{and } H) = \frac{\tilde{E}(\text{and } \tilde{H})}{m_x \tilde{\omega}_x^2 \tilde{x}_0^2},$$

$$\alpha = \tilde{\alpha}\tilde{x}_0\sqrt{\frac{m_x}{m_y}},$$

we obtain the symmetric mode coupling (SMC) Hamiltonian,

$$H_{\text{SMC}} = T + V_{\text{SMC}} = -\frac{g^2}{2}\left(\frac{\partial^2}{\partial x^2} + \frac{\partial^2}{\partial y^2}\right) + \frac{1}{8}(x-1)^2$$
$$\times (x+1)^2 + \frac{\omega_y^2}{2}[y + \alpha(x^2-1)]^2, \tag{19}$$

where g plays the role of $\hbar$. This model has two minima at $(x,y) = (\pm 1, 0)$ and one saddle point at $(0, \alpha)$; the y coordinates of the two minima are the same and are shifted from the coordinate of the saddle point. The barrier height, i.e., the potential difference between the saddle point and the minima, is normalized to be $1/8 = 0.125$. The frequency in y direction is always $(\partial^2 V_{\text{SMC}}/\partial y^2)^{1/2} = \omega_y$, while that in x direction at the minima is normalized to unity. The potential contour is depicted in Fig. 4 for $(\omega_y, \alpha) = (0.5, 1)$. This model has been used as a typical example of multidimensional tunneling in many fields.[20,7] Especially, in the case of the proton tunneling in malonaldehyde, the coordinate x mainly represents the motion of the hydrogen atom transferring from O to O, while y roughly represents the scissors like motion of the O–C–C–C–O frame [see Fig. 5(a)]. Since the mutual approach of the two oxygen atoms makes tunneling more probable, the saddle point $(0, \alpha)$ is located not at $y = 0$, but at positive y. The parameters of malonaldehyde determined by Bosch et al.[20] are $(\omega_y, \alpha, g) = (0.48, 1.7, 0.10)$ in the present notations. For a general case that the a_1 symmetric mode (as a nonrigid molecule)[25] couples to the tunneling coordinate to assist the hydrogen tunneling, Eq. (19) gives one of the simplest models among those which keep the symmetry of the system.

Although the SMC model is already quite simple, sometimes it is more convenient to use the following simpler model (V-parabola model) which has the similar characteris-

TABLE II. Energy splittings of the symmetric mode coupling (19) calculated quantum mechanically for vibrationally excited states. Parameter g is equal to 0.04.

(ω_y,α)	(0.8,1.0)	(0.3,0.22222)
$\Delta E_{0,0}^a$	4.6(-9)[b]	2.33(-8)
$\Delta E_{0,1}$	122.8(-9)	3.07(-8)
$\Delta E_{0,2}$	1671.1(-9)	3.93(-8)
$\Delta E_{0,3}$	15301.1(-9)	4.93(-8)
Tunneling regions	I–I	C–C

[a]$\Delta E_{0,n}$ indicates the energy splitting for the state in which the vibrational motions are in the ground and the nth excited levels for the tunneling direction and the direction transversal to it, respectively.

[b]Figures in parentheses are the power of ten by which the entry is to be multiplied.

tics of potential topography to that of SMC. This is parabolic both in the left-($x<0$) and in the right-hand ($x>0$) side,

$$H_{VP}=T+V_{VP} \qquad (20)$$

with

$$V_{VP}(x,y)=\tfrac{1}{2}\omega_s^2 s^2+\tfrac{1}{2}l^2,$$

where the kinetic energy operator T is the same as Eq. (19) and

$$\begin{pmatrix} s \\ l \end{pmatrix}=\begin{pmatrix} \cos\theta & -\sin\theta \\ \sin\theta & \cos\theta \end{pmatrix}\begin{pmatrix} x\pm 1 \\ y \end{pmatrix}. \qquad (21)$$

Here, the sign $+(-)$ is taken in the left- (right-hand) side. Roughly speaking, the parameter θ plays the same role as the coupling strength α in the SMC model. Since this potential is separable in each side, we can easily analyze the characteristics of tunneling. We should remember, however, that this potential has a cusp along y axis and thus is a little bit pathological. The essential conclusions are not affected, though.

First, with use of the SMC model (19), quantum mechanical calculations of tunneling energy splitting have been carried out for a variety of parameters. Here, only the following two representative examples are shown (see Table II): (1) the intermediate coupling case where tunneling mainly goes through the I region [Fig. 6(a) of the paper I] and (2) the weak coupling case where tunneling mainly goes through the C region [Fig. 6(b) of the paper I]. In the first example (left-hand column), vibrational excitation promotes the tunneling very much. This can be simply attributed to the decrease of the Gamow factor Θ in the WKB theory [see Eqs. (3) and (4)]. As mentioned before, this is not a surprising but a common phenomenon just like in the one-dimensional case. The right-hand column shows that the tunneling through the C region is also promoted by the vibrational excitation. The promotion is weak, simply because the coupling is weak. Namely, no qualitative difference between the tunnelings through the I region and C region region can be found in the SMC model.

The similar feature can be seen in Fig. 6, in which the energy splittings (in logarithmic scale) for vibrationally ground and excited states of the V-parabola model are plotted as a function of θ. In both ends of $\theta(\sim0°$ and $\sim90°)$, mixed tunneling contributes mainly, while pure tunneling dominates in the middle. In either case, however, tunneling is found to
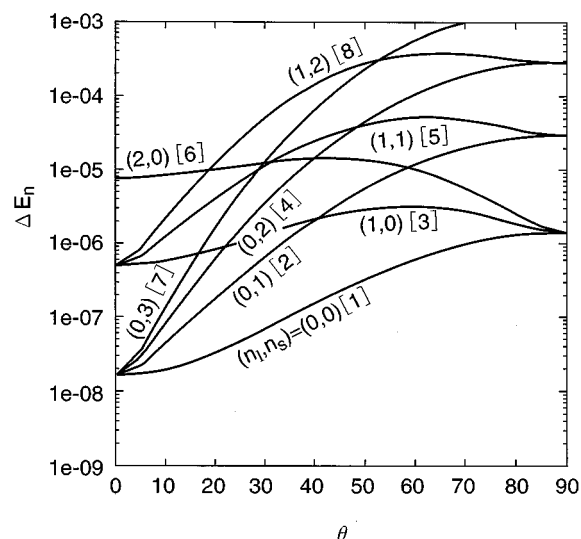

FIG. 6. Tunneling energy splitting (in logarithmic scale) of the V-parabola model (20) by the exact quantum mechanical calculation as a function of the coupling parameter θ. Parameters (ω_s,g) are equal to (0.7,0.06).

be promoted by vibrational excitation. Another interesting feature seen from Fig. 6 is mode specificity of tunneling: The energy splitting is not necessarily a monotonically increasing function of the total excitation energy (the numbers in the square brackets in Fig. 6 represent the order in total excitation energy). In the left-hand side, and excitation in n_l mode is more effective than that in n_s mode. This is because the former coincides with the tunneling direction. The opposite tendency is seen in the right-hand side as can be easily conjectured from Eq. (21).

It is of great interest to see how the tunneling path is affected by vibrational excitation when the tunneling mainly
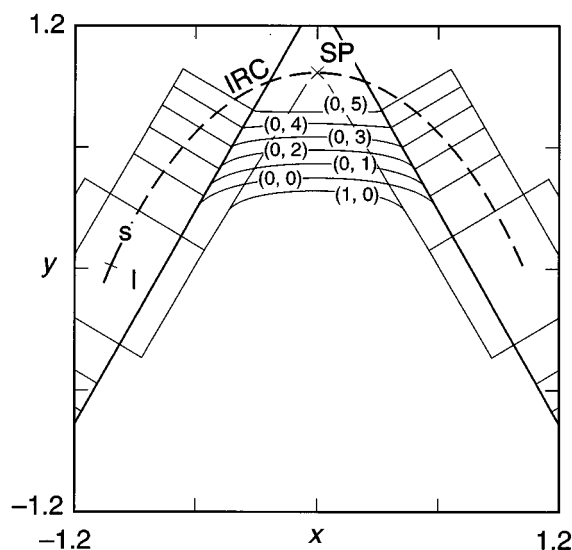

FIG. 7. Tunneling paths for several vibrationally excited states in the case of the V-parabola model (20). Parameters are chosen to be $(\omega_s,\theta,g)=(0.42,30°,0.04)$. (n_l,n_s) specifies the vibrational quantum numbers of l and s modes.

TABLE III. Energy splittings of the symmetric mode coupling (19). Left-(right)-hand column is the result by exact quantum mechanical calculation [by the sudden approximation (15)]. Parameters (ω_y, α, g) are equal to (0.2,0.25,0.04).

	EQM	Sudden
$\Delta E_{0,0}$	2.36(-8)	2.18(-8)
$\Delta E_{0,1}$	2.60(-8)	1.88(-8)
$\Delta E_{0,2}$	2.85(-8)	1.26(-8)
$\Delta E_{0,3}$	3.10(-8)	1.00(-8)

TABLE IV. Energy splittings of the antisymmetric mode coupling (22) calculated quantum mechanically. Parameter g is equal to 0.04.

(ω_y, β)	(0.5,1)	(0.2,0.3)
$\Delta E_{0,0}$	1.4(-10)	182.1(-10)
$\Delta E_{0,1}$	60.5(-10)	5.7(-10)
$\Delta E_{0,2}$	1316.5(-10)	85.0(-10)
$\Delta E_{0,3}$	18920.0(-10)	117.9(-10)
$\Delta E_{0,4}$		113.9(-10)
$\Delta E_{0,5}$		88.7(-10)
Tunneling regions	I–I	C–C

goes through the I region. Figure 7 shows this for several vibrational states in the case of the V-parabola model with parameters $(\omega_s, \theta, g) = (0.42, 30°, 0.04)$. As is seen from Fig. 7, the tunneling paths are strongly dependent on vibrational state. The numbers in the parenthesis (n_l, n_s) on each path represent the vibrational quantum numbers in the l and s mode, respectively. All the tunneling paths take shortcuts compared to the IRC. More important, vibrational excitation in the s mode makes tunneling path closer to the IRC, while that in the l mode shifts it inward: the two modes have opposite effects in a sense. This kind of significant mode specificity of tunneling can be understood naturally, but is found for the first time in this calculation as far as the authors know. This is in nice contrast to Fig. 7 of Ref. 15, where the instanton path is not state specific and changes in a monotonic way as a function of temperature.

Finally, let us investigate the validity of the adiabatic and sudden approximations. If we apply the adiabatic approximation Eq. (8) to the SMC model, the energy splitting becomes independent of the vibrational quantum number n_y, whatever ω_y is: The adiabatic potential has the same shape as that of $n_y=0$, since the frequency in y direction is constant. This is not in agreement with the exact quantum results except when the coupling α is zero. Table III compares the energy splittings calculated by the sudden approximation with the exact results. In the sudden approximation, $\Delta E_{n_x}^{1D}(y)$ in Eq. (15) is calculated by the WKB formula Eq. (3). We notice that the energy splitting by the sudden approximation decreases with vibrational excitation, while the exact one increases. Thus, neither the adiabatic nor the sudden approximation is reliable for investigating the tunneling in excited states of the SMC model.

B. Case of antisymmetric mode coupling

The antisymmetric mode coupling (ASMC) Hamiltonian is defined by

$$H_{\text{ASMC}} = T + V_{\text{ASMC}} = -\frac{g^2}{2}\left(\frac{\partial^2}{\partial x^2} + \frac{\partial^2}{\partial y^2}\right) + \frac{1}{8}(x-1)^2$$

$$\times (x+1)^2 + \frac{\omega_y^2}{2}(y - \beta x)^2, \quad (22)$$

where g and ω_y have the same meanings as those of the SMC model (19) and β represents the coupling strength. This can be obtained by scaling all the quantities in the same way as in the SMC model. A potential contour map is given in Fig. 7 of paper I (γ there is equal to $\gamma = \omega_y^2 \beta$). There are two

minima at $(x,y) = (\pm 1, \pm \beta)$ and one saddle point at $(x,y) = (0,0)$; these two minima are shifted in y direction. The barrier height is again normalized to be $1/8 = 0.125$. In the case of malonaldehyde, the coordinate x again represents the motion of transferring hydrogen, while y may represent the antisymmetric C–O stretching mode [Fig. 5(b)].

In the same way as in the SMC model, the following simpler shifted parabola model is introduced:

$$\hat{H}_{\text{SP}} = \hat{T} + V_{\text{SP}}(x,y) \quad (23)$$

with

$$V_{\text{SP}}(x,y) = \begin{cases} \frac{1}{2}(x+1)^2 + \frac{1}{2}\omega_y^2(y+y_0)^2 & \text{for } x<0 \\ \frac{1}{2}(x-1)^2 + \frac{1}{2}\omega_y^2(y-y_0)^2 & \text{for } x\geq 0. \end{cases}$$

(The potential map is depicted in Fig. 15 of the paper I.) The parameter y_0 plays the role of coupling strength.

With use of the ASMC model (22), the tunneling energy splittings have been calculated quantum mechanically for a wide range of parameters. Among them, two distinct cases with different characteristics of tunneling are found. The numerical results are shown in Table IV. The left-hand column represents the first case where tunneling mainly passes through the I region [Fig. 3(a)], while the right-hand column corresponds to the other case where tunneling mainly goes through the C region [Fig. 3(b)]. This has essentially the same feature as in the case of the shifted parabola potential given in Table 15 of paper I: pure tunneling in the I region is always promoted by vibrational excitation, while mixed tunneling in the C region is either promoted or suppressed by the excitation. As for the former case, the promotion of tunneling is attributed to the decrease of the Gamow factor in the same way as in the SMC model.

In the case of mixed tunneling, the energy splitting oscillates with respect to n_y and is sensitive to the parameter β. This is definitely different from the case of SMC. This oscillatory change occurs because the excited vibrational wave functions have nodal lines in the C region (nearly parallel to the x axis) and thus the overlap integral in Herring's formula (2) can oscillate due to the phase cancellation. In order to confirm this conjecture, vibrational wave functions are depicted in Fig. 8 for the parameters $(\omega, \beta, g) = (0.2, 0.3, 0.04)$. Here, $\Psi_{(0,5)}^L$ drawn in the negative x side ($\Psi_{(0,5)}^R$ drawn in the positive x side) is the wave function localized in the left (right) half. The nodal lines of the left-hand wave function are shifted down compared to that of the right-hand wave function. Actually, the energy splitting $\Delta E_{(0,5)}$ is relatively
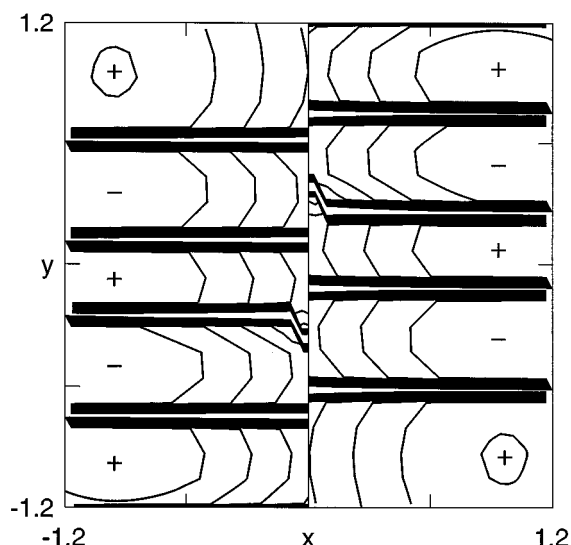
FIG. 8. Contour map of the wave functions $\Psi^L_{(0,5)}$ (left-half) and $\Psi^R_{(0,5)}$ (right-half) in the case of the ASMC model (22). Parameters and interval of the contours are chosen to be $(\omega_y, \beta, g) = (0.2, 0.3, 0.04)$ and 1.0.

small as is seen in Table IV. The same feature can be seen in the model (23): Fig. 9 shows the energy splitting $\Delta E_{(n_x, n_y)}$ (in logarithmic scale) as a function of the shift y_0 for the case $(\omega, g) = (0.7, 0.07)$. It should be noted that tunneling occurs mainly through the C region when $y_0 \lesssim y_{cr} = \sqrt{(2n_y + 1)g/\omega_y}$ (for instance, $y_{cr} = 0.707$ when $n_y = 2$), while through the I region when $y_0 \gtrsim y_{cr}$. As is seen from Fig. 9, the energy splitting oscillates as a function of y_0 when and only when the tunneling goes through the C region. Moreover, the number of dips is the same as the vibrational quantum number n_y. These results confirm the mechanism of oscillation in the right-hand column of Table IV.

Finally, we touch upon the adiabatic and sudden approximations in the present model. In the same way as in the case of SMC model, the adiabatic approximation Eq. (8) leads to
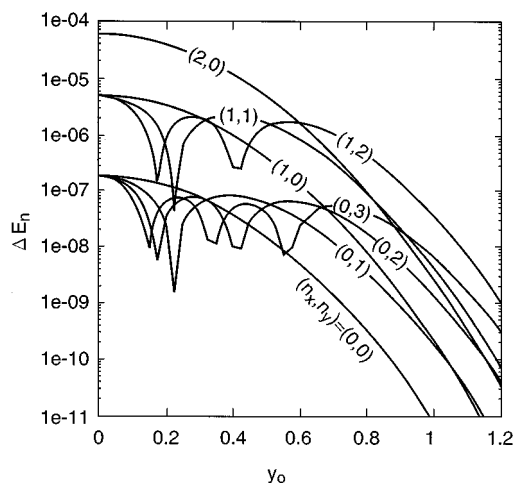
FIG. 9. Tunneling energy splitting (in logarithmic scale) of the shifted parabola model as a function of y_0. Parameters are chosen to be $(\omega_y, g) = (0.7, 0.07)$.
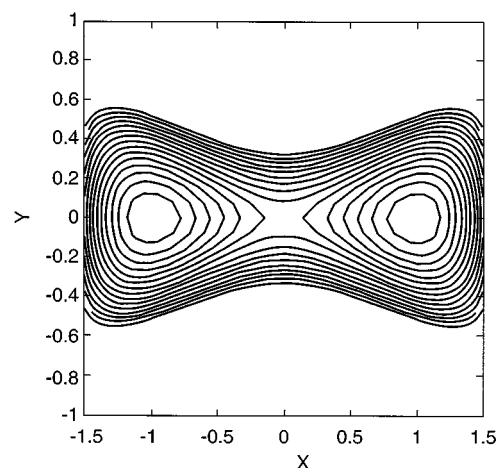
FIG. 10. Contours of Sqz potential [Eq. (24)] for the parameters $(\omega_y, \gamma) = (1.5, 1)$. The other conditions are the same as in Fig. 4.

the energy splitting independent of n_y. This does not exhibit any characteristic behavior discussed above and can never be reliable. If we try to apply the sudden approximation Eq. (15), we encounter a problem: Since the potential curve in x direction is not symmetric except when y is zero. Thus, we cannot use Eq. (15) directly anymore.

C. Case of squeezed double well potential

As a third example, we consider a model which is symmetric with respect to x axis. The squeezed double well (Sqz) Hamiltonian,

$$H_{Sqz} = T + V_{Sqz} = -\frac{g^2}{2}\left(\frac{\partial^2}{\partial x^2} + \frac{\partial^2}{\partial y^2}\right) + \frac{1}{8}(x-1)^2$$

$$\times (x+1)^2 + \frac{1}{2}[\omega_y^2 - \gamma(x^2-1)]y^2,$$

(24)

is such an example. Here, g and ω_y have the same meaning as those of SMC model (19) and γ represents the coupling strength. Two minima at $(x,y) = (\pm 1, 0)$ and one saddle point at $(x,y) = (0,0)$ are located on x axis. The barrier height is again normalized to be $1/8 = 0.125$. The local frequency $\Omega_y(x)$ along y axis is defined as $\Omega_y^2(x) = \omega_y^2 - \gamma(x^2-1)$ and thus the coupling parameter γ plays a role of squeezing (positive γ) and spreading (negative γ) the potential in y direction. Figure 10 depicts the potential contour for the case $(\omega_y, \gamma) = (1.5, 1)$. It should be noted that when $\omega_y^2 > -\gamma$, this potential has additional saddle points at $(\pm\sqrt{1 + \omega_y^2/\gamma}, \pm\omega_y/\sqrt{2}|\gamma|)$ and drops beyond these points. Thus, we cannot take a very large positive γ so as to keep the double well topography. A typical example of the Sqz potential can be found also in malonaldehyde, in which y coordinate now corresponds to an out-of-plane wagging motion depicted schematically in Fig. 5(c). Since the stable structure of malonaldehyde is planar and the out-of-plane deviation makes O–O distance larger, the topography of PES should be represented by the squeezed double well model. It should be noted that this Sqz model is not the same as that of paper I.

TABLE V. Energy splittings of the Sqz potential (24) calculated with use of the exact quantum mechanical method (EQM) and the sudden approximation (sudden). Parameters (ω_y, γ, g) are equal to $(0.2, 0.05, 0.05)$.

Method	EQM	Sudden
$\Delta E_{0,0}$	6.12(−7)	6.01(−7)
$\Delta E_{0,1}$	3.99(−7)	4.08(−7)
$\Delta E_{0,2}$	3.31(−7)	3.07(−7)
$\Delta E_{0,3}$	3.04(−7)	2.49(−7)
$\Delta E_{0,4}$	3.03(−7)	2.14(−7)
$\Delta E_{0,5}$	3.09(−7)	1.90(−7)

Here we have slightly modified the latter which has a bit too strong coupling near the well and may not be a good model for typical molecular vibration.

In the same way as before, the following simpler squeezed parabola (Sqz-P) potential is introduced:

$$H_{\text{Sqz-P}} = T + v_{\text{Sqz-P}}(x) + \frac{1}{2}\,\Omega_y^2(x)y^2 \qquad (25)$$

with

$$v_{\text{Sqz-P}}(x) = \begin{cases} \frac{1}{2}(x+1)^2 & \text{for } x<0 \\ \frac{1}{2}(x-1)^2 & \text{for } x\geq 0 \end{cases},$$

$$\Omega_y(x) = \begin{cases} \omega_y & \text{for } |x|>X \\ \omega_{\text{Sqz}} & \text{for } |x|\leq X \end{cases}.$$

In this model, the frequency in y direction is switched at $|x|=X$ to produce the squeezing (when $\omega_{\text{Sqz}}>\omega_y$) or the spreading effect (when $\omega_{\text{Sqz}}<\omega_y$). This can create a strong squeezing, while, as mentioned above, it cannot be made by the Sqz potential Eq. (24) because of the additional saddle points.

Exact quantum mechanical calculations have been done for a wide range of parameters in the case of Sqz potential. Table V shows tunneling energy splittings of vibrationally excited states for a representative parameter. The following features can be found in Table V: (i) vibrational excitation in y direction suppresses tunneling when vibrational quantum number n_y is small ($n_y \leq 4$ in the present case), (ii) the amount of suppression by the excitation decreases with n_y, and (iii) the splitting starts to increase from a certain n_y ($n_y=5$ in the present case). In the sudden regime $\omega\ll 1$, the feature (i) can be understood intuitively based on the sudden approximation (15): As the n_y increases, the wave function $\phi_{n_y}(y)$ spreads and the population near the x axis decreases. On the other hand, $\Delta E^{1D}(y)$ decreases rapidly as $|y|$ increases, since the potential is squeezed in y direction. Thus, the Franck–Condon integral in Eq. (15) is expected to decrease as n_y increases. Actually, the energy splittings by the sudden approximation given in the right-hand column of Table V shows the suppression of the tunneling by vibrational excitation in y direction.

In order to investigate the other features (ii) and (iii), we made quantum mechanical calculations of energy splitting for the Sqz-P potential. Figure 11 shows the energy splitting as a function of the squeezed frequency ω_{Sqz}. The other parameters are fixed at $(\omega_y, X, g) = (0.4, 0.5, 0.07)$. At $\omega_{\text{Sqz}}=0.4$,

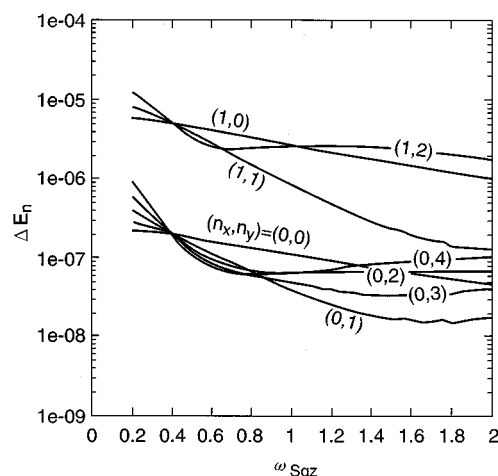

FIG. 11. Tunneling energy splitting (in logarithmic scale) of the squeezed parabola model (25) as a function of ω_{Sqz}. Parameters are chosen to be $(\omega_y, X, g) = (0.4, 0.5, 0.07)$.

the potential is separable and thus energy splitting is independent of n_y. For a weakly squeezed case ($0.4 < \omega_{\text{Sqz}} < 0.7$), the energy splitting decreases as n_y increases. On the other hand, for a strongly squeezed case ($\omega_{\text{Sqz}} > 0.8$), the splitting is not a monotonic function of ω_{Sqz} but changes quite randomly. This irregular behavior starts at smaller ω_{Sqz} for larger n_y. Moreover, we confirmed that when ω_y is small, the regular behavior is preserved in wide range of ω_{Sqz}. This is probably because the sudden regime becomes more appropriate at small ω_y. It can also be seen in Fig. 11 that the energy splitting increases monotonically as n_y increases in the case of spread potential ($\omega_{\text{Sqz}} < 0.4$). This is not surprising and can be understood easily by the sudden approximation (15) in the same way as above.

In the adiabatic regime in which ω_y is larger than unity, the same feature as above can be basically found. There has been found, however, an interesting exception noted below. Table VI gives energy splittings in the Sqz potential for a small γ (left-hand and central columns) and for a large γ (right-hand column). In the case of small coupling γ, we found that the tunneling is, as expected, suppressed by the vibrational excitation. This can be interpreted if we employ the adiabatic approximation Eq. (8): The tunneling dynamics can be understood in terms of the renormalized potential (see Fig. 10 of paper I). From this, we can predict that the energy splitting is diminished by the vibrational excitation in y direction. Actually, the energy splittings estimated by the adiabatic approximation (8) (central column) agree quite well

TABLE VI. Energy splittings of the Sqz potential (24) with large ω_y. The parameter g is equal to be 0.05.

(ω_y, γ) Method	(1.8,0.1)		(1.5,0.5)
	EQM	Adiabatic	EQM
$\Delta E_{0,0}$	7.16(−7)	6.92(−7)	5.57(−7)
$\Delta E_{0,1}$	6.45(−7)	6.24(−7)	3.01(−7)
$\Delta E_{0,2}$	5.84(−7)	5.63(−7)	83.7(−7)

with those of quantum mechanical calculation (left-hand column). As γ increases (right-hand column of Table VI), this suppression disappears and irregular behavior comes out in the same way as in the discussions of Fig. 11. Another significantly different feature appears when the Fermi resonance between the $(0,n_y)$ and (n_x',n_y') states occurs with nonzero n_x': The tunneling splitting itself is found to disappear in this case. Since the state with higher n_x has larger amplitude in the potential barrier region, an admixture of the state (n_x',n_y') in the state $(0,n_y)$ crucially affects the energy splitting of the latter state, even if the admixture is very small.

IV. PROTON TUNNELING IN TROPOLONE

A. Available experimental data

As was mentioned in Sec. I, quite a few experimental data on tropolone molecule are now available. The electronically ground state $\tilde{X}\,^1A_1$ has been studied by infrared spectroscopy,[30,31] FT-microwave spectroscopy,[35] and single vibronic level fluorescence (SVLF) spectroscopy.[24,32,27] IR spectra give us information about normal modes. The FT-microwave spectroscopy can directly observe the tunneling energy splitting of the $\tilde{X}$ state. The SVLF spectra provide us with the relation between the vibronic level in the excited state $\tilde{A}$ and that in the ground state $\tilde{X}$. For the first electronically excited state $\tilde{A}\,^1B_2$, the UV absorption spectra[22] and the laser fluorescence excitation spectra[23–25,27] have been measured. The latter have also been measured for the ($^{18}O/^{16}O$ and D/H) isotope substituted tropolone.[26,28,29] The data obtained from the laser fluorescence excitation spectra include the main information we are interested in; namely, the accurate energy levels of various vibrationally excited states in $\tilde{A}$.

Theoretical study by the *ab initio* MO method has been done by Redington and Bock for $\tilde{X}$ state,[34] while no data on the excited state is available. They calculated (1) the optimized geometry and the saddle point geometry by the restricted Hartree–Fock (RHF) method with 6-31G** basis set, (2) the energy difference between these two points by the second-order Møller–Plesset (MP2) perturbation method with the 6-31G* basis set, and (3) thirty-nine normal modes and their frequencies by the RHF method with 6-31G basis set. Since the level of computation is high enough for the qualitative understanding, there is little room to doubt the obtained geometries and characteristics of normal modes, although the barrier height and the normal mode frequencies may involve non-negligible errors.

Our main interest consists in the proton tunneling in the $\tilde{A}$ state, because more interesting data on tunneling splittings have been measured for $\tilde{A}$ state. The direct information of tunneling energy splitting is obtained by combining the laser fluorescence excitation spectroscopy and the FT-microwave spectroscopy. As is shown in Fig. 1, the laser fluorescence excitation spectra for jet-cooled tropolone give us the values of $|\Delta E_n' - \Delta E_0''|$, where ′ and ″ represent the $\tilde{A}$ and $\tilde{X}$ states, respectively; for instance, $\Delta E_n''$ is the energy splitting of the vibrational state $\mathbf{n}$ in the electronic state $\tilde{X}$. Since the $\Delta E_0''$ is determined to be 0.974 cm^{-1} from the FT-microwave spectra,[35] we can have an estimate of $\Delta E_n'$. In order to con-

TABLE VII. Observed tunneling energy splittings $\Delta E_n'$ of tropolone $\tilde{A}$ state.

Band	TRNOH[a]	TRNOD[b]	Assignment	Symm[d]
0^0	20	2	Origin	
11^1	14	c	C–C stretch	a_1
12^1	18	2	CCC bend	a_1
13^1	33	3	CC–O/CCC deform	a_1
14^1	31	11	in-plane ring deform	a_1
14^2	29	13		
19^2	10	c	out-of-plane bend	a_2
25^2	5		out-of-plane bend	b_1
26^2	8	c	out-of-plane bend	b_1
26^4	6			
26^6	5			
26^8	2			
26^{10}	c			
26^{12}	c			
$14^1 26^2$	5	2		
$25^1 26^1$	c	c		

[a]References 25, 27, and 35.
[b]Reference 27. Here, $\Delta E_0''$ is assumed to be zero.
[c]Unresolved.
[d]Irreducible representation of C_{2V} point group. Tropolone is considered to be nonrigid. These assignments are due to Ref. 31.

firm that the splitting in the spectra is really caused by tunneling, they measured the temperature dependence of the intensity ratio and the effects of isotope substitution on the splitting.

The vibrational modes in the $\tilde{A}$ state can be assigned indirectly. For the ground state $\tilde{X}$, using the results of infrared spectra and MO calculation, we can assign each vibrational mode. The correspondence between the modes of $\tilde{X}$ state and $\tilde{A}$ state is established by using the SVLF spectra. Combining these data, we can guess the characteristics of the vibrational modes in the $\tilde{A}$ state. The tunneling energy splittings $\Delta E_n'$ observed and assigned in this way are listed in Table VII, where TRNOH (TRNOD) represents tropolone (tropolone in which -OH is deuterated to -OD). Many interesting features can be found: (1) excitation of the ν_{12}' mode does not affect significantly the tunneling, (2) excitation of the mode ν_{13}' and that of ν_{14}' promote the tunneling, (3) excitation of the mode ν_{25}' and that of ν_{26}' suppress the tunneling, and so on. The fundamental vibrational frequencies are shown in Table VIII both for the $\tilde{X}$ and $\tilde{A}$ states.

TABLE VIII. Vibrational fundamentals in the $\tilde{X}$ and the $\tilde{A}$ states of tropolone.

Mode	Symmetry[a]	$\tilde{X}$[b]	$\tilde{A}$[c]
11	a_1	739	511
12	a_1	674	640
13	a_1	434	414
14	a_1	359	296
19	a_2	271	269
25	b_1	177	171
26	b_1	109	39

[a]These assignments are due to Ref. 31.
[b]Data from the SVLF spectra (Ref. 27).
[c]Data from the laser fluorescence excitation spectra (Ref. 27).

TABLE IX. (A) Optimized geometries (in Å) of both the stable structure and the saddle point structure of tropolone in $\tilde{X}$ state by MP2 method with 6-31G** basis set. (B) Bond length (in Å) of both the stable structure and the saddle point structure of tropolone in $\tilde{X}$ state by MP2 method with 6-31G** basis set in comparison with the RHF method (Ref. 34).

(A)

	Stable structure			Saddle point		
Atom	x	y	z	x	y	z
1 C	−1.139	0.141	0.000	0.736	−0.814	0.000
2 C	0.000	1.074	0.000	−0.736	−0.814	0.000
3 C	1.360	0.825	0.000	−1.598	0.296	0.000
4 C	2.033	−0.410	0.000	−1.259	1.644	0.000
5 C	1.510	−1.689	0.000	0.000	2.251	0.000
6 C	0.148	−2.066	0.000	1.259	1.644	0.000
7 C	−0.988	−1.288	0.000	1.598	0.296	0.000
8 O	−2.276	0.687	0.000	1.153	−2.040	0.000
9 O	−0.410	2.349	0.000	−1.153	−2.040	0.000
10 H	−1.396	2.247	0.000	0.000	−2.461	0.000
11 H	1.972	1.720	0.000	−2.651	0.042	0.000
12 H	3.115	−0.341	0.000	−2.102	2.327	0.000
13 H	2.226	−2.501	0.000	0.000	3.335	0.000
14 H	−0.033	−3.136	0.000	2.102	2.327	0.000
15 H	−1.942	−1.803	0.000	2.651	0.042	0.000

(B)

	Stable structure		Saddle point	
Parameter	RHF	MP2	RHF	MP2
$C_1=O$	1.212	1.261	1.263	1.295
C_2-O	1.330	1.340	1.263	1.295
$O\cdots O$	2.525	2.499	2.252	2.307
OH	0.952	0.991	1.204	1.228
C_1C_2	1.488	1.473	1.490	1.472
C_2C_3	1.345	1.383	1.386	1.405
C_3C_4	1.432	1.407	1.386	1.390
C_4C_5	1.345	1.382	1.386	1.398
C_5C_6	1.433	1.413	1.386	1.398
C_6C_7	1.345	1.377	1.386	1.390
C_7C_1	1.452	1.437	1.386	1.405
C_3H	1.076	1.084	1.075	1.083
C_4H	1.077	1.084	1.077	1.085
C_5H	1.075	1.083	1.075	1.083
C_6H	1.077	1.085	1.077	1.085
C_7H	1.075	1.084	1.075	1.083

B. MO calculation and tunneling dynamics of $\tilde{X}$ state

Although our main interest consists in the proton tunneling in $\tilde{A}$ state, we start with that in $\tilde{X}$ state because the accurate information of PES for $\tilde{X}$ can be obtained by the *ab initio* MO calculation.

We have made a MO calculation of the $\tilde{X}$ state using the GAUSSIAN 92 program package:[43] The MP2 method with 6-31G** basis set is employed to calculate the energy, the fully optimized geometries, thirty-nine normal modes, and their frequencies both at the stable structure and at the saddle point structure. The energy is also calculated by MP4(SDQ) method with 6-31G** basis set at the stable and saddle point structures to get more accurate estimate of the energy barrier. Table IX lists the geometries of both the stable structure and the saddle point structure. Comparing with the geometries by RHF method, we can see that electron correlation lengthens

the double bonds and shortens the single bonds in the seven-membered ring. The other single bonds become longer than those of RHF. These are well-known tendencies and can be explained by the fact that electron correlation mixes anti-bonding orbital with bonding orbital and weakens the bonding.

Frequencies and characteristics of the normal modes are summarized in Tables X and Fig. 12. It can be seen from Tables X(A) and X(B) that most of the frequencies by the MP2 method are smaller than those of RHF (see Table IV of Ref. 34). This is also well known and comes from the same reason as above. For the modes with 1200–1600 cm^{-1}, the correspondences between computed frequencies and measured ones are not very clear. Decomposition of the normal modes ν'' at the stable structure in terms of those ($\nu^{\ddagger}$) at the saddle point are given in Table X(C); Each normal mode

TABLE X. Computed normal mode frequencies and characteristics in the $\tilde{X}$ state of tropolone. (A) Normal mode frequencies (cm^{-1}) at the stable structure. (B) Normal mode frequencies (cm^{-1}) at the saddle point structure. (C) Decomposition of some representative normal modes at the stable structure in terms of those at the saddle point structure.

(A)

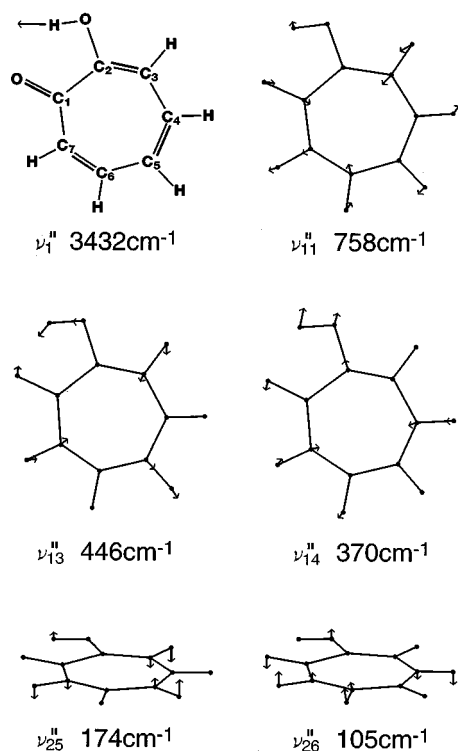| ν'' [a]	Symm	Calc	Obs[b]	ν'' [a]	Symm	Calc	Obs[b]
(1)	A'	3432	3121	(21)	A'	899	875
(2)	A'	3266	3055	11(22)	A'	758	741
(3)	A'	3259	3055	12(23)	A'	706	674
(4)	A'	3256	3030	(24)	A'	547	551
(5)	A'	3240	3023	13(25)	A'	446	434
(6)	A'	3231	3006	14(26)	A'	370	359
(7)	A'	1717	1635	(27)	A'	355	349
(8)	A'	1677	1628	(28)	A''	977	1000
(9)	A'	1641	1565	(29)	A''	942	983
(10)	A'	1597	1522	(30)	A''	914	908
(11)	A'	1552	1499	(31)	A''	850	828
(12)	A'	1497	1481	(32)	A''	806	774
(13)	A'	1474	1470	(33)	A''	757	751
(14)	A'	1379	1460	(34)	A''	641	720
(15)	A'	1344	1427	(35)	A''	524	676
(16)	A'	1302	1412	(36)	A''	385	335
(17)	A'	1263	1274	19(37)	A''	351	272
(18)	A'	1261	1252	25(38)	A''	173	177
(19)	A'	1094	1146	26(39)	A''	105	110
(20)	A'	989	952				

(B)

$\nu^{\ddagger}$	Symmetry	Calc	$\nu^{\ddagger}$	Symmetry	Calc
1	a_1	3267	21	b_2	1444
2	a_1	3260	22	b_2	1318
3	a_1	3232	23	b_2	1293
4	a_1	2097	24	b_2	1120
5	a_1	1716	25	b_2	778
6	a_1	1613	26	b_2	568
7	a_1	1483	27	b_2	365
8	a_1	1437	28	a_2	970
9	a_1	1266	29	a_2	842
10	a_1	991	30	a_2	653
11	a_1	897	31	a_2	381
12	a_1	747	32	a_2	147
13	a_1	725	33	b_1	1240
14	a_1	416	34	b_1	948
15	b_2	1323i	35	b_1	919
16	b_2	3264	36	b_1	758
17	b_2	3238	37	b_1	530
18	b_2	1772	38	b_1	378
19	b_2	1654	39	b_1	171
20	b_2	1535			

(C)

Mode (stable)	Modes (saddle point)	Symmetry
$\nu_1''(1)$	$0.69\nu_{15}^{\ddagger} + 0.65\nu_4^{\ddagger}$	$b_2 + a_1$
$\nu_{11}''(22)$	$0.96\nu_{25}^{\ddagger}$	b_2
$\nu_{12}''(23)$	$0.92\nu_{13}^{\ddagger}$	a_1
$\nu_{13}''(25)$	$0.78\nu_{14}^{\ddagger} + 0.54\nu_{12}^{\ddagger}$	a_1
$\nu_{14}''(26)$	$0.66\nu_{27}^{\ddagger} + 0.49\nu_{14}^{\ddagger} + 0.49\nu_{12}^{\ddagger}$	$a_1 + b_2$
$\nu_{19}''(37)$	$0.84\nu_{31}^{\ddagger} + 0.53\nu_{38}^{\ddagger}$	$a_2 + b_1$
$\nu_{25}''(38)$	$0.96\nu_{39}^{\ddagger}$	b_1
$\nu_{26}''(39)$	$0.95\nu_{32}^{\ddagger}$	a_2

[a]Figures in the parentheses are those by Redington and Bock (Ref. 34).
[b]Data from Refs. 22, 27, 30, 31, and 32.

FIG. 12. Normal modes of tropolone in the $\tilde{X}$ state.

TABLE XII. Parameters of the three-dimensional model (26) for the tropolone $\tilde{X}$ state.

Parameter	Value
g	0.0732
ω_y	0.469
α	1.19
ω_z	0.0446
γ	0.00190

On the basis of these calculations, we construct a model PES for the proton tunneling in the $\tilde{X}$ state. It is natural to expect that the vibrational modes which largely affect the tunneling are basically the same for the $\tilde{X}$ and $\tilde{A}$ states. Thus, we choose the direct tunneling mode, ν''_{13} mode and ν''_{26} mode as relevant coordinates for a three-dimensional model. The other modes are regarded as irrelevant ones although their zero point energies (ZPE) are added to the model PES. Since ν''_{13} is assigned to a_1 symmetry, the coupling should be that of the SMC potential. On the other hand, ν''_{26} is the out-of-plane wagging motion and thus the potential in this direction should be squeezed. On the basis of these considerations, we propose the following model PES:

$$H = -\frac{g^2}{2}\left(\frac{\partial^2}{\partial x^2} + \frac{\partial^2}{\partial y^2} + \frac{\partial^2}{\partial z^2}\right) + \frac{1}{8}(x-1)^2(x+1)^2$$

$$+ \frac{\omega_y^2}{2}[y + \alpha(x^2-1)]^2 + \frac{1}{2}[\omega_z^2 - \gamma(x^2-1)]z^2, \quad (26)$$

where modes x and z represent the direct tunneling mode and ν''_{26} mode, respectively. The mode y collectively represents the coupling of a_1 mode and largely includes ν''_{13} mode. We believe that the essential topography of the relevant part of PES of tropolone is correctly represented by this simple model, although the quantitative accuracy may not be enough.

The parameters in Eq. (26) are determined from the data obtained above. First of all, we need to remove the translational and rotational degrees of freedom. To do this, let $\mathbf{X}_P$ ($P = L, R, C$, or S, where L and R represent the left and right stable structures, respectively, C is the midpoint of L and R, and S is the saddle point structure) be the $3N$-dimensional mass-weighted coordinate vector representing P in xy plane. First, we take the origin of coordinates at the center of mass. Second, the R structure ($\mathbf{X}_R$) is rotated around z axis such that $|\mathbf{X}_L - \mathbf{X}_R|$ becomes minimal. Then, we define $\mathbf{X}_C \equiv (\mathbf{X}_L + \mathbf{X}_R)/2$. Finally, the S structure is rotated around z axis such that $|\mathbf{X}_S - \mathbf{X}_C|$ becomes minimal. The potential parameters are determined as described below. (i) α represents the distance ratio $\overline{SC}/\overline{LC}$ and can be determined straightforwardly. (ii) Frequencies Ω_x in x direction and Ω_y in y direction can be determined from the expressions,

$$\Omega_x^2 = \sum_i \langle LC|i\rangle^2 \nu''^2_i, \quad (27)$$

$$\Omega_y^2 = \sum_i \langle SC|i\rangle^2 \nu''^2_i, \quad (28)$$

vector at the ν'' is expressed by the linear combination of those at the $\nu^{\ddagger}$ and major components are picked up in Table X. It should be noted here that the right-most column shows not the symmetry of the nonrigid molecule but that of $\nu^{\ddagger}$ contributing to the corresponding ν''. The following interesting features can be found: (1) Symmetries of the ν''_{11} and ν''_{26} are b_2 and a_2, respectively, which are different from those assigned by experiments. We note that even if ν''_{11} is b_2 like mode (as a rigid molecule), a pair of eigenstates splitted by the tunneling have a_1 and b_2 symmetries and thus the selection rule does not change. (2) Modes ν''_1, ν''_{14}, and ν''_{19} are composed of $\nu^{\ddagger}$'s with different symmetries. These new assignments will be essential for understanding the tunneling dynamics. Finally, the energy differences between the stable and the saddle point structures are given in Table XI for several different calculation methods.

TABLE XI. Energies (kcal mol^{-1}) at the saddle point of $\tilde{X}$ relative to the energy of the stable structure. The 6-31G** basis set are used for all calculations.

Calculation	No ZPE	With ZPE[a]	With ZPE'''[b]
MP2	5.31	7.99	7.96
MP3[c]	9.22		
MP4(DQ)[c]	9.93		
M4(SDQ)[c]	8.86	11.54	11.51

[a]All the zero point energies (ZPE) except for that along the direct tunneling mode are taken into account.
[b]All the ZPE except for those along the direct tunneling mode, the ν_{13} mode, and the ν_{26} mode are taken into account.
[c]Geometry and ZPE are taken from the calculation of the MP2 method.

TABLE XIII. Energy splittings (cm^{-1}) calculated with use of the exact quantum mechanical method (EQM) for the model potential (26) of tropolone.

	EQM
$\Delta E_{0,0,0}$[a]	1.05
$\Delta E_{0,0,1}$	0.965
$\Delta E_{0,0,2}$	0.887
$\Delta E_{0,0,3}$	0.819
$\Delta E_{0,0,4}$	0.758
$\Delta E_{0,0,5}$	0.705
$\Delta E_{0,0,6}$	0.656
$\Delta E_{0,1,0}$	7.61
$\Delta E_{0,1,1}$	7.02

[a]Subscripts represent vibrational quantum numbers of the direct tunneling mode, ν_{13} mode (approximately), and ν_{26} mode.

where $\langle LC|i\rangle$ ($\langle SC|i\rangle$) represents the component of the ν_i'' mode in $\mathbf{X}_{LC}$ direction (that of the ν_i'' mode in $\mathbf{X}_{SC}$ direction). Frequency ratio ω_y is then obtained as Ω_y/Ω_x. (iii) Since the normal mode vector of ν_{26}'' is almost identical to that of $\nu_{32}^{\ddagger}$, we can easily determine ω_z and γ: the ν_{26}'' frequency ($=105.2$ cm^{-1}) at L and that ($=147.2$ cm^{-1}) at S correspond to ω_z and $\sqrt{\omega_z^2+\gamma}$, respectively. (iv) g is determined such that the energy barrier ($=11.51$ kcal mol^{-1}) including the ZPE corresponds to 1/8. Parameters determined in this way are listed in Table XII. We note that no parameter was fitted to reproduce any energy splitting.

Tunneling energy splitting has been calculated quantum mechanically with this three-dimensional Hamiltonian (26) using the DVR method. Numbers of grids used here are 60, 40, and 40 for x, y, and z coordinates, respectively. Table XIII gives the energy splittings for several vibrational states. First, the energy splitting ΔE_0 of the ground state is 1.05 cm^{-1}, which is in good agreement with the observed value ($=0.974$ cm^{-1}). It may be fair to say that this agreement is somewhat accidental because the present model is simple and the tunneling energy splitting is known to be very sensitive to PES. The more important thing is the dependence of $\Delta E_\mathbf{n}$ on $\mathbf{n}$. It can be seen that the vibrational excitation in z direction suppresses the tunneling weakly, while that in y direction promotes it quite strongly: The modes y and z play the same role as those in the two-dimensional (2D) SMC and Sqz models discussed in the previous section. This supports the conjecture that the 2D models in the previous section may be directly used to understand the effects of vibrational excitation in the case of the dimension higher than 2.

C. Interpretation and discussion on $\tilde{A}$ state

On the basis of the numerical analysis done in Sec. III and the previous subsection, here we try to analyze the experimental data on proton tunneling in the $\tilde{A}$ state. As is clarified in Sec. III, the symmetry of PES is a crucial factor to understanding the effects of vibrational excitation on tunneling. In order to know the symmetry of the PES of the $\tilde{A}$ state, information on the stable structure and the characteristics of normal modes are required. Since no reliable *ab initio*

MO calculation of $\tilde{A}$ state has been reported so far, we try to interpret the available experimental data from our present knowledge.

Let us first consider the effects of ν_{13}' and ν_{14}'. Since the former has a_1 symmetry, the symmetry of the PES should be that of the SMC model (19), in which x and y correspond to the direct tunneling coordinate and ν_{13}' mode, respectively. According to the numerical results shown in Tables II and XIII, the excitation of this mode is thus expected to promote the tunneling. Experimentally, the first excitation of ν_{13}' gives the energy splitting of 33 cm^{-1} (3 cm^{-1}) compared to the splitting of 20 cm^{-1} (2 cm^{-1}) of the vibrationally ground state in the case of TRNOH (TRNOD). Our prediction qualitatively agrees with this experimental data. If we assume that the ν_{14}' mode is similar to the ν_{14}'', it has both a_1 and b_2 components. The first excitation of ν_{14}' promotes the tunneling, which can be explained by the SMC model. The excitation by two quanta in this mode of TRNOH, however, suppresses the tunneling slightly from the first excited state. This is probably because ν_{14}' has the b_2 component and the PES has coupling of the ASMC type.

If we assume that the ν_{11}' has the same symmetry (b_2) as the ν_{11}'', the symmetry of the PES should be that of the ASMC model (22). Thus, the suppression of the tunneling by the ν_{11}' excitation can be understood by the out-of-phase cancellation in Herring's formula. Unfortunately, long excitation progression of this mode has not been observed yet. As emphasized in Sec. III, excitation of this mode is expected to give an oscillatory behavior of the energy splitting as a function of the vibrational quantum number. This, if possible, can be considered as an experimental observation of *mixed tunneling*.

In Table VII, the long progression of the ν_{26}' mode has been observed and the corresponding energy splitting decreases monotonically with its excitation. To know the symmetry of PES, we need information on the normal mode. It has been repeatedly pointed out[32,27] that the strong Duschinsky effect between the ν_{25} mode and the ν_{26} mode is found in the $\tilde{X}$–$\tilde{A}$ electronic spectra. Namely, the ν_{26}' normal mode of $\tilde{A}$ state mainly consists of the mixture of the ν_{25}'' and the ν_{26}'' modes of $\tilde{X}$ state. Since the reliable MO calculations for the normal modes ν_{25}'' and ν_{26}'' are available (depicted schematically in Fig. 12), the ν_{26}' mode can be guessed to include the antisymmetric wagging motion of two O atoms. Therefore, the deviation of the ν_{26}' mode from planar structure makes O–O distance larger and thus makes the barrier height of the proton tunneling between the two O atoms larger. This clearly indicates the existence of squeezing effect in the PES. If we assume that the stable structure is planar in $\tilde{A}$ state, the PES must be symmetric with respect to the deviation of the ν_{26}' mode. Thus, the ν_{26}' mode coupled with the tunneling coordinate may be described by the Sqz or the Sqz-P model, in which x and y correspond to the direct tunneling mode and to the ν_{26}' mode, respectively. It should be noted that ν_{26}' is the mode with the lowest frequency 39 cm^{-1}, while the direct tunneling mode has the frequency of about 3000 cm^{-1}. Thus, this case definitely fits to the sudden regime. The numerical results for the Sqz model shown in Table V and the model for the $\tilde{X}$ state [Eq. (26)] shown in Table XIII

should qualitatively be in accordance with the experimental finding. In Table VII, other two modes ν'_{19} and ν'_{25} with the symmetries different from a_1 have the same tendency as that of ν'_{26}. This again indicates that the symmetry of coupling is important to clarify the effect of vibrational excitation on tunneling.

In the above analysis, however, one subtle question has not been paid attention to. The stable structure of the $\tilde{A}$ state might be bent and thus C_{2V} symmetry group might not be appropriate. Roughly speaking, the following two opposite effects compete with each other in determining whether a molecule with conjugated π electrons prefers planar structure or not; reduction of the overlap between adjacent atoms makes the structure bent as is seen in the cyclohexane molecule, while the conjugated π electrons prefer planar structure as is seen in the ground state benzene. As is mentioned above, the *ab initio* MO calculation and x-ray diffraction data have shown that the structure of the $\tilde{X}$ state is planar. This is because the effect of conjugated π electrons is stronger than that of avoiding the overlapping. For the $\pi-\pi^*$ excited state $\tilde{A}$, however, this situation can be different; the effect of the conjugated π electrons should become weaker. Unfortunately, however, neither direct observation nor any MO calculation has been done to answer this question. The SVLF spectra seem indirectly to support the planar structure. If the stable structure is not planar, we need to consider both the squeezing effect and the effect of antisymmetric mode coupling for clarifying the effect of ν'_{26}.

Redington *et al.*[26] interpreted the effect of the ν'_{26} mode based on the adiabatic viewpoint. They introduced the (T,τ) two-dimensional PES, in which T and τ represent the direct tunneling coordinate and an out-of-plane twisting mode, respectively. The latter is considered to be responsible for reorganizing the ν'_{26} mode, since the ν'_{26} mode need to be rearranged during the proton transfer. Moreover, they assumed that this two-dimensional surface $V_v(T,\tau)$ is different for each vibrational quantum number v of the ν'_{26} mode; namely they used the adiabatic approximation. As mentioned above, however, the frequency of the ν'_{26} mode is two orders of magnitude smaller than that of the direct tunneling mode and thus the adiabatic approximation cannot be allowed.

V. CONCLUSION

We have investigated the effects of vibrational excitation on tunneling using several model systems: Tunneling energy splittings of excited states are obtained by the exact quantum mechanical calculation and are interpreted by the WKB theory and the sudden and adiabatic approximations. Various interesting effects are found: (1) In the case of the SMC model, vibrational excitation always promotes tunneling. (2) In the case of ASMC, pure tunneling in I region is promoted by the excitation, while mixed tunneling in C region is either promoted or suppressed. The latter is attributed to the phase cancellation in the overlap integral of Herring's formula. (3) In the case of squeezed potential, vibrational excitation suppresses the tunneling when the squeezing effect is sufficiently weak, while strong squeezing makes the tunneling irregular.

Next, the proton tunneling dynamics of tropolone has been studied based on the above numerical analysis. First, a model PES of the ground state $\tilde{X}$ has been constructed with use of the high accuracy *ab initio* MO calculation and the energy splitting has been calculated on this PES. Then, the experimentally observed energy splitting of the first excited state $\tilde{A}$ has been interpreted; promotion by the excitation of ν'_{13}, suppression by the excitation of ν'_{11}, and suppression by the excitation of ν'_{26} have been explained by the SMC model, the ASMC model, and the Sqz model, respectively. It has been emphasized that the symmetry of the coupled vibrational mode is responsible for the topography of the PES and the latter plays a key role in the tunneling dynamics of vibrationally excited states.

Note added in proof. After this paper was accepted for publication, we received a preprint by Benderskii, Grebenshchikov, and Mil'nikov in which they reproduced oscillatory behavior of energy splitting in the ASMC case by using an instantonlike treatment (private communication).

[1] Special issue on *Tunneling in Chemical Reactions*, edited by V. A. Benderskii, V. I. Goldanskii, and J. Jortner [Chem. Phys. **170**, 265 (1993)]; V. A. Benderskii, D. E. Makarov and C. A. Wight, Adv. Chem. Phys. **88**, 1 (1994); J. Jortner and B. Pullman, *Tunneling* (Reidel, Dordrecht, 1986); B. Chance, D. C. Devault, H. Frauenfelder, R. A. Marcus, J. R. Schrieffer, and N. Sutin, *Tunneling in Biological Systems* (Academic, New York, 1979).
[2] T. Banks, C. M. Bender, and T. T. Wu, Phys. Rev. D **8**, 3346 (1973); T. Banks and C. M. Bender, *ibid.* **8**, 3366 (1973).
[3] J. L. Gervais and B. Sakita, Phys. Rev. D **16**, 3507 (1977).
[4] S. Coleman, in *The Whys of Subnuclear Physics*, edited by A. Zichichi (Plenum, New York, 1979).
[5] C. G. Callan, Jr. and S. Coleman, Phys. Rev. D **16**, 1762 (1977).
[6] J. P. Sethna, Phys. Rev. B **24**, 692 (1981).
[7] A. Auerbach and S. Kivelson, Nucl. Phys. B **257** [FS14], 799 (1985).
[8] N. Takigawa, K. Hagino, M. Abe, and A. B. Balantekin, Phys. Rev. C **49**, 2636 (1994).
[9] T. F. George and W. H. Miller, J. Chem. Phys. **56**, 5722 (1972); **57**, 2458 (1972).
[10] R. A. Marcus and M. E. Coltrin, J. Chem. Phys. **67**, 2609 (1977).
[11] M. Ya. Ovchinnikova, Chem. Phys. **36**, 85 (1979).
[12] V. K. Babamov and R. A. Marcus, J. Chem. Phys. **74**, 1790 (1981); H. Nakamura and A. Ohsaki, *ibid.* **83**, 1599 (1985); H. Nakamura, Chem. Phys. Lett. **141**, 77 (1987); A. Ohsaki and H. Nakamura, *ibid.* **142**, 37 (1987).
[13] B. C. Garrett, D. G. Truhlar, A. F. Wagner, and T. H. Dunning, Jr., J. Chem. Phys. **78**, 4400 (1983).
[14] D. G. Truhlar, A. D. Isaacson, and B. C. Garrett, *Theory of Chemical Reaction Dynamics*, edited by M. Baer (Chemical Rubber, Boca Raton, 1985), Vol. 4.
[15] V. A. Benderskii, D. E. Makarov, and P. G. Grinevich, Chem. Phys. **170**, 275 (1993).
[16] S. Takada and H. Nakamura, J. Chem. Phys. **100**, 98 (1994), this is referred to as ''paper I'' in this article.
[17] S. Takada and H. Nakamura, Supp. Prog. Theor. Phys. **116**, 295 (1994).

[18] T. Carrington, Jr. and W. H. Miller, J. Chem. Phys. **84**, 4364 (1986).

[19] N. Shida, P. F. Barbara, and J. E. Almlöf, J. Chem. Phys. **91**, 4061 (1989).

[20] E. Bosch, M. Moreno, J. M. Lluch, and J. Bertrán, J. Chem. Phys. **93**, 5685 (1990).

[21] S. L. Baughcum, Z. Smith, E. B. Wilson, and R. W. Duerst, J. Am. Chem. Soc. **106**, 2260 (1984); P. Turner, S. L. Baughcum, S. L. Coy, and Z. Smith, *ibid*. **106**, 2265 (1984).

[22] A. C. P. Alves and J. M. Hollas, Mol. Phys. **23**, 927 (1972); **25**, 1305 (1973).

[23] R. Rossetti and L. E. Brus, J. Chem. Phys. **73**, 1546 (1980).

[24] Y. Tomioka, M. Ito, and N. Mikami, J. Phys. Chem. **87**, 4401 (1983).

[25] R. L. Redington, Y. Chen, G. J. Scherer, and R. W. Field, J. Chem. Phys. **88**, 627 (1988).

[26] R. L. Redington, T. E. Redington, M. A. Hunter, and R. W. Field, J. Chem. Phys. **92**, 6456 (1990).

[27] H. Sekiya, Y. Nagashima, and Y. Nishimura, J. Chem. Phys. **92**, 5761 (1990); Bull. Chem. Soc. Jpn. **62**, 3229 (1989).

[28] H. Sekiya, K. Sasaki, Y. Nishimura, Z. Li, A. Mori, and H. Takeshita, Chem. Phys. Lett. **173**, 285 (1990).

[29] H. Sekiya, Y. Nagashima, T. Tsuji, Y. Nishimura, A. Mori, and H. Takeshita, J. Phys. Chem. **95**, 10311 (1991).

[30] Y. Ikegami, Bull. Chem. Soc. Jpn. **34**, 94 (1960); **36**, 1118 (1963).

[31] R. L. Redington and T. E. Redington, J. Mol. Spectrosc. **78**, 229 (1979).

[32] A. C. P. Alves, J. M. Hollas, H. Musa, and T. Ridley, J. Mol. Spectrosc. **109**, 99 (1985).

[33] R. L. Redington, J. Chem. Phys. **92**, 6447 (1990).

[34] R. L. Redington and C. W. Bock, J. Phys. Chem. **95**, 10284 (1991).

[35] K. Tanaka, H. Honjyo, T. Tanaka, H. Takaguchi, Y. Ohshima, and Y. Endo, Abstracts of the Meeting of the Molecular Structure, Yokohama, Japan, 1991 (unpublished), p. 223.

[36] V. A. Benderskii, S. Yu. Grebenshchikov, E. V. Vetoshkin, G. V. Mil'nikov, and D. E. Makarov, J. Phys. Chem. **98**, 3300 (1994); V. A. Benderskii, S. Yu. Grebenshchikov, G. V. Mil'nikov, and E. V. Vetoshkin, Chem. Phys. **188**, 19 (1994); V. A. Benderskii, S. Yu. Grebenshchikov, and G. V. Mil'nikov, *ibid*. (submitted).

[37] C. Herring, Rev. Mod. Phys. **34**, 631 (1962).

[38] L. D. Landau and E. M. Lifshitz, *Quantum Mechanics* (Pergamon, Oxford, 1975).

[39] V. P. Maslov and M. V. Fedoriuk, *Semi-Classical Approximation in Quantum Mechanics* (Reidel, Dordrecht, 1981).

[40] M. Wilkinson, Physica. D **21**, 341 (1986).

[41] K. Fukui, J. Phys. Chem. **74**, 4161 (1970); K. Fukui, S. Kato, and H. Fujimoto, J. Am. Chem. Soc. **97**, 1 (1975).

[42] J. C. Light, I. P. Hamilton, and J. V. Lill, J. Chem. Phys. **82**, 1400 (1985); R. M. Whitnell and J. C. Light, *ibid*. **90**, 1774 (1989).

[43] GAUSSIAN 92, Revision A. M. J. Frisch, G. W. Trucks, M. Head-Gordon, P. M. W. Gill, M. W. Wong, J. B. Foresman, B. G. Johnson, H. B. Schlegel, M. A. Robb, E. S. Replogle, R. Gomperts, J. L. Andres, K. Raghavachari, J. S. Binkley, C. Gonzalez, R. L. Martin, D. J. Fox, D. J. Defrees, J. Baker, J. J. P. Stewart, and J. A. Pople, Gaussian, Inc., Pittsburgh PA, 1992.